Efficient hydrogen production from irradiated aluminum hydroxides

Josiane Kaddissy, Stéphane Esnouf, Dimitri Saffré, Jean-Philippe Renault

Efficient hydrogen production from irradiated Aluminum Hydroxides

Josiane A. Kaddissy [a†], Stéphane Esnouf [b], Dimitri Saffré [c§], Jean-Philippe Renault[a]

[a] LIONS, NIMBE, CEA, CNRS, Université Paris Saclay, F-91191 Gif-sur-Yvette Cedex, France
[b] DEN-Service d'Etude du Comportement des Radionucléides (SECR), CEA, Université Paris-Saclay, F-91191, Gif-sur-Yvette, France
[c] Orano TNI, 1 rue des Hérons, 78180 Montigny Le Bretonneux, France
[†] Current adress: Orano, Tour Areva, 1 Pl. Jean-Millier, 92400 Courbevoie 78180 Montigny Le Bretonneux
[§] Current adress: ANDRA, Parc de la Croix Blanche, 1-7, rue jean-Monnet, 92298 Chatenay-Malabry cedex

Abstract

Radiation-catalysis is a well-known process leading to H_2 production through radiolysis of adsorbed water on oxides. In this article, we show that common, easily accessible, hydroxides can be as much efficient for H_2 production as the more efficient oxide identified until now.

H_2 radiolytic yields were determined from the same nanostructured hydrated samples that differ by their particle size (AlOOH L and AlOOH S for large and small particle size, respectively). The measured yields are of the order of 10^{-8} mol. J^{-1}. It means that such an irradiated material produces more efficiently H_2 than an equivalent mass of water. H radicals, trapped electrons (F centers), and related O^- centers were identified by electron paramagnetic resonance (EPR), at room and low temperature. Adsorbed water seems to play a role in the secondary processes of radical recombination, allowing a very efficient H_2 production in these systems. This raises interesting questions about the energy transfer mechanism underlying this efficient hydrogen production and provide design lines for the design of efficient radiation-catalytic materials for H_2 production.

Keywords: Radiolysis, Irradiation, Radiation catalysis, Hydrogen, defects, EPR, Aluminum hydroxides.

1. Introduction

Hydrogen produced by water radiolysis in the vicinity of radioactive rocks, has been a major source of energy for development of life on the early earth. [1] In today's world, it may be important to sustain deep subsurface microbial communities in rock fractures.[2, 3] In fact, some minerals have been known since the sixties to facilitate radiolytic processes by the so called radiation catalysis.[4, 5] The observation of radio-catalytic H_2 production on oxides has triggered many hopes concerning the possibility of radiolytically powered fuel cells.[6] In these

studies, the reference material is ZrO_2, with yields as high as 150 molecules for 100eV absorbed by adsorbed water [7, 8] but Al_2O_3, SIO_2 and TiO_2 may also be quite effective. [9-11]
Such high yields have of course fostered in turn the development of various technological schemes for harvesting radiation in order to produce H_2.[12, 13] [14-16]
For a while, the radio-catalysis on oxide surfaces has been interpreted as an exciton migration from the bulk of the material, devoid of hydrogen, to the surface hydroxyl/water groups that act as energy traps.[6, 17] Direct electron injection from the oxide to the surface water has also been identified.[4]
In this short communication, we present data on a very efficient radiolytic H_2 production on the surface of nanostructured aluminum oxyhydroxides (AlOOH). AlOOH (Boehmite) is formed as a corrosion product during aluminum oxidation, but it is also prepared on an industrial scale by wet processes as a precursor of alumina. It was here selected as a model compound for other hydroxides and oxyhydroxides.

2. Materials & Methods

This part was detailed in our previous work [18].

2.1 Sample preparation and characterization

All oxyhydroxides samples AlOOH (Boehmite) were acquired from Sasol®, Germany and were in the highest purity available. AlOOH was studied in two different crystallite sizes (named AlOOH S and AlOOH L for small and large particles, respectively). They have already been extensively characterized in reference [18], and additional information are shown in the SI (Figure, S1, S2, S3 and S4).
Samples were placed into humidity chambers, which contain various saturated salt solutions to generate desired levels of relative humidity, denoted as RH, water uptake was evaluated by weighing each sample periodically.
Lithium chloride purchased from Sigma Aldrich with a reference number 746460-100G, Potassium carbonate purchased from Sigma Aldrich with a reference number 791776-100G and Sodium chloride purchased from Sigma Aldrich with a reference number S9625-500G were used in order to obtain relative humidity of 11, 44 and 76 % at room temperature consequently.[19, 20]
Thermogravimetric measurements (TGA) were performed with a Mettler-Toledo TGA/DSC. Samples dedicated to H_2 quantification were irradiated in Pyrex ampules evacuated at 10^{-2} mbar, filled with 0.8 mbar of ultrahigh purity helium gas and then sealed.
Concerning samples dedicated to EPR analysis, Room temperature EPR sample cells were standard NMR tubes evacuated and flame-sealed.Though, samples dedicated to low temperature EPR, also irradiated at low temperature were irradiated in EPR cold finger quartz Dewar. Samples irradiated for low temperature EPR were made into pellets. It was essential to irradiate in the same vessel and analyze by EPR without creating irradiation defects in the zone analyzed by the EPR. The pellet is irradiated while it is hanged to the wire and once irradiated it

is released to the bottom of the dewar where it is supposed to be analyzed by EPR as detailed in [21]. Dewars are filled with liquid nitrogen in order to keep the samples irradiated at 77 K.
EPR measurements were conducted at Laboratoire National Henri Becquerel (LNHB), CEA-Saclay, France and Laboratoire des Solides Irradiés (LSI), Ecole Polytechnique, France. Spectra were acquired on X-Band EMX Bruker spectrometers (X-Band) with a 100 Hz field modulation. In most cases microwave power and amplitude modulation were 10 mW, 0.2 mT, respectively. The microwave frequency was measured with a frequency counter. Quantification was estimated using a hydroxyl-TEMPO sample (4-hydroxy-2,2,6,6-Tetramethylpiperidyne 1 oxyl) as a standard. The error on the conversion factor is estimated at 25%.

2.2 Irradiation experiments

Electron beam irradiations were conducted using a linear accelerator located in NIMBE, Saclay, France. The pulse-width was 10 ns, the electron energy was 10 MeV and the repetition rate was 5 Hz. No sample heating was detected. The typical dose delivered per pulse determined using the Fricke dosimeter was: 28 Gy/pulse.[22, 23]
L-α-alanine EPR dosimetry was used to determine the dose delivered in the EPR tubes and Dewars irradiated with electron beams.
Most of the samples irradiated using electron beam dedicated to analyzing molecular H_2 were placed in 10 mL Pyrex ampules with valves. Only the bottom of the ampule was irradiated and was conceived to have a spherical homogeneous shape. The preliminary washing of the ampules was optimized to reduce as far as possible the hydrogen production of the empty ampules.

2.3 H_2 determination

Hydrogen released from hydrated samples irradiated using electron beam was analyzed using μ-GC (μGC-R3000 SRA instrument) (NIMBE) and Agilent 450 (LRMO) using ultrahigh purity argon (argon 6.0) as the carrier gas. A calibration curve is obtained using standard gas mixture with various concentrations of H_2 (from 100 to 1000 ppm).

2.4 Correspondance between the relative humidity and the number of water layers

The number of water layer on AlOOH surface was calculated using a specific surface of 40 m^2/g for AlOOH L, and of 270 m^2/g for AlOOH S, and a surface occupied by water of 5 m^2/mg. [24]

3. Results and Discussion

In a dry state, AlOOH nanoparticles of 18 nm of diameter (named hereafter AlOOH L for Large) have radiolytic yields in the range of $(0.05\pm0.02)\times10^{-7}$ mol/J.[18] When minute amount of water is added to the system (1% in mass, which represents less than one adsorbed water layer, see SI), this yield, calculated with respect to the total energy received by the system, reaches

(7.6±0.2)x10^{-8} mol/J (Figure 1). It means that such a material produces more efficiently H_2 than an equivalent mass of water. In fact, when these H_2 yields are expressed with respect to the energy directly received by the adsorbed water, as it is done currently for oxide systems, they take a leap to 134x10^{-7}mol/J or 129 molecules/100 eV. (Table S1).

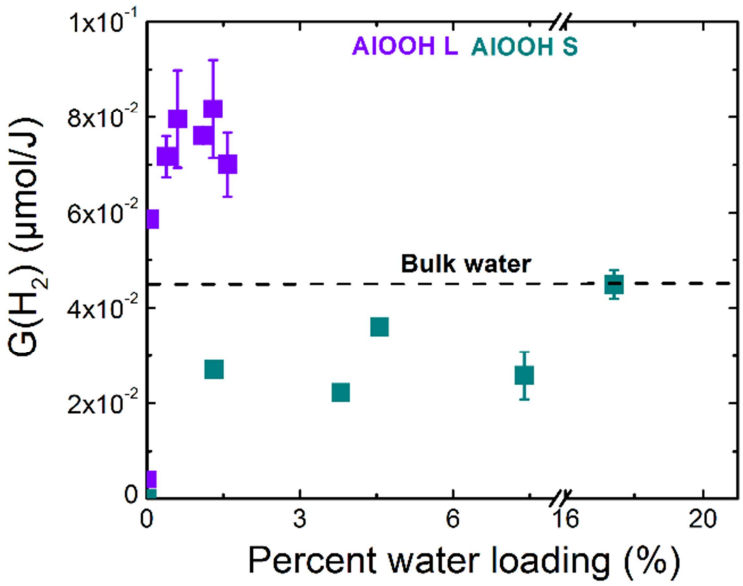

Figure 1. Hydrogen production from electron-irradiated AlOOH L and S with respect to water loading. Violet squares (AlOOH L). Cyan blue squares (AlOOH S). Black dotted line: primary radiolytic yield of liquid water.

These values are comparable to the ones measured from ZrO_2, and, higher than the one obtained for CPG glasses.[25] To achieve such high yields, a total transfer of energy captured by the system to water and a facilitated OH bond dissociation are both required.

Interestingly, these yields (Figure 1, Figure S6 and Table S1) are lower for smaller particles, (5nm, named hereafter AlOOH S). This result is quite surprising considering that smaller sizes are usually expected to favor both energy transfer processes and water adsorption (AlOOH S adsorbs ten times more water than AlOOH L see Figure S5).[17]

This raises interesting questions about the energy transfer mechanism underlying this efficient hydrogen production. Luckily, in materials like hydroxides, some reactive species can remain trapped in the solid network. Therefore, we identified by electron paramagnetic resonance (EPR) the defect patterns (Figure 2 and Table S2) i.e. various types of radicals produced after irradiation in dry (no adsorbed water detectable in thermogravimetric analysis (TGA)) and hydrated conditions (76% relative humidity which corresponds to 1.7% in mass of adsorbed water for AlOOH L and 17% in mass of water for AlOOH S) (Figure S5).

For the oxidative part, O^- and O_3^- species can be observed in hydrated (Figure 3) and dry conditions.[21] The EPR g factors of these defects are not modified by the hydration.

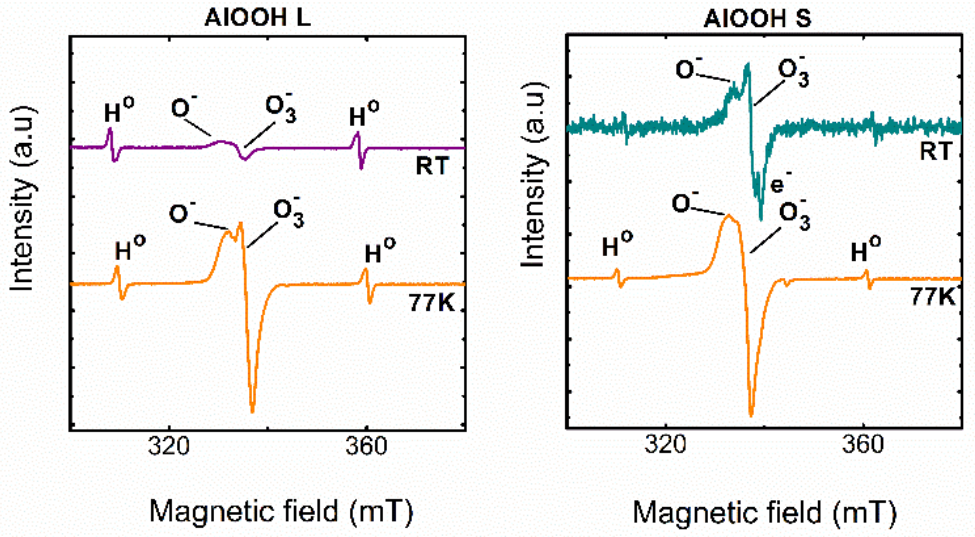

Figure 2. EPR spectra of electron irradiated at 46 kGy of AlOOH L (left) and AlOOH S (right). Two spectra for each sample are shown, one irradiated and analyzed at RT and the second irradiated and analyzed at 77 K.

The spectra recorded and irradiated at room temperature (RT) are compared to that recorded and irradiated at 77K (Figure 2). The noise is higher in AlOOH S because of its higher water content. Spectra are normalized with respect to the mass of samples.
O^- is a primary species in the ionization process, produced either by homolytic dissociation

$$Al\cdots OH^- \rightarrow Al\cdots O^- + H^\circ \quad \text{Equation 1}$$

or by ionization

$$Al\cdots OH^- \rightarrow Al\cdots OH + e^- \rightarrow Al\cdots O^- + H^+ \text{ (locally trapped by hydroxide)} + e^- \quad \text{Equation 2}$$

The concentration in O^- saturates with the dose, probably because it transforms progressively into O_3^-. (Figure 3)

The reaction that conducted to the formation of superoxide center or ozonide radical are recalled below:

$$O^- + O^- = O_2^{2-} \quad \text{Equation 3}$$

$$O_2^{2-} + \text{hole} = O_2^- \quad \text{Equation 4}$$

$$O_2^- + O^- = O_3^- + e^- \quad \text{Equation 5}$$

Ozonide radical was also observed in Barium hydroxides [26] and in different oxides such as quartz.[27] The following reactions have been also proposed:

$$O_2^{2-} + O_2^- = O_3^- + O^{2-} \quad \text{Equation 6}$$

Of course, this radical can also be produced by dissociation of O_2, but we have no signature of O_2 production in our systems (i.e. pure H_2 is produced):

$$O_2 = O + O \quad \text{Equation 7}$$

$$O + O_2 = O_3 \quad \text{Equation 8}$$

$$O_3 + e = O_3^- \quad \text{Equation 9}$$

Regardless of particle size, the hydration slightly decreases O^- production (Table 1). However, even in the hydrated case, the yields of O^- remain important and are stoichiometric with respect to H_2 yields presented in Table 1 (O^- carries one oxidative equivalent whereas H_2 molecule carries two). It is thus tempting to see in O^- the oxidative counterpart to H_2 production, its lower production upon hydration being due to the opening of additional dissipative/recombination pathways.

Table 1. Radiolytic yields in 10^{-8} mol/J calculated with respect to the energy received by the total system.

	AlOOH L hydrated 77K	AlOOH L hydrated RT	AlOOH L dry RT	AlOOH S hydrated 77K	AlOOH S hydrated RT	AlOOH S dry RT
AlO°	70±10	16±4	23±5	80±20	4±0.5	13±3
AlO_3°	17±4	0.3 - 1.9	0.7±0.1	18±5	0.3±0.03	0.4±0.1
H_2	ND	8±1	0.3* (1.2 trapped)	ND	2 - 4	0* (0.46 trapped)

ND : not determined , RT room temperature, * data from [18]

For the reductive species, two putative precursors of H_2, H atoms and thermalized electron are observed, in EPR (Figure 2) as trapped defects. H atom doublet, separated by 50 mT is seen having an EPR g factor of 2.013 (Figure 2, AlOOH L and to a lesser extent AlOOH S). The trapped electron defect is identified only in AlOOH S as a singlet with an EPR g factor of 1.998.[6] We must notice that yields cannot be extracted from this data, as the concentration in these defects saturates very quickly with the dose (Figure 3).

Trapped H atoms and electrons have been previously observed in dry AlOOH L ([21] and Figure 3), H atoms in the bulk of the material, and electrons on the surface. In the same AlOOH L material, but hydrated, only H atoms are present, with EPR properties and concentration similar to the dry material which suggests an internal localization of these species. In this case, the hydration destabilizes the electrons on the surface and may favor their recombination to produce hydrogen.

In AlOOH S, the concentrations in H atoms and electrons are much smaller than in large particles and appear only in the hydrated state (Figure 2 and 3). Water is obviously not expected to stabilize such defects at room temperature. However, its effect may be indirect, by favoring the diffusion of the species out of their production site and thus limiting the recombination effect by confinement observed in small dry particles [18, 21] or by thermalizing them more efficiently than the surrounding material. As an alternative pathway, we can consider that these species come from the direct lysis of water on the surface and are subsequently injected in the material. In fact, the amount of adsorbed water is much higher in AlOOH S than in AlOOH L. The isotope labelling experiments that would allow to distinguish between these two hypotheses are prevented by the long equilibrium time required to control the hydration.

We must also notice that, in these two pathways, water helps/allows the production of defects within the neighboring material. This observation converges with recent researches on H_2 injection in copper from neighboring water radiolysis.[28] We must also notice that this defect accumulation does not affect the structural properties of the materials (see SI, Figures S7 and S8).

In a second time, low temperature irradiations were used to stabilize and quantify the primary species produced by irradiation.

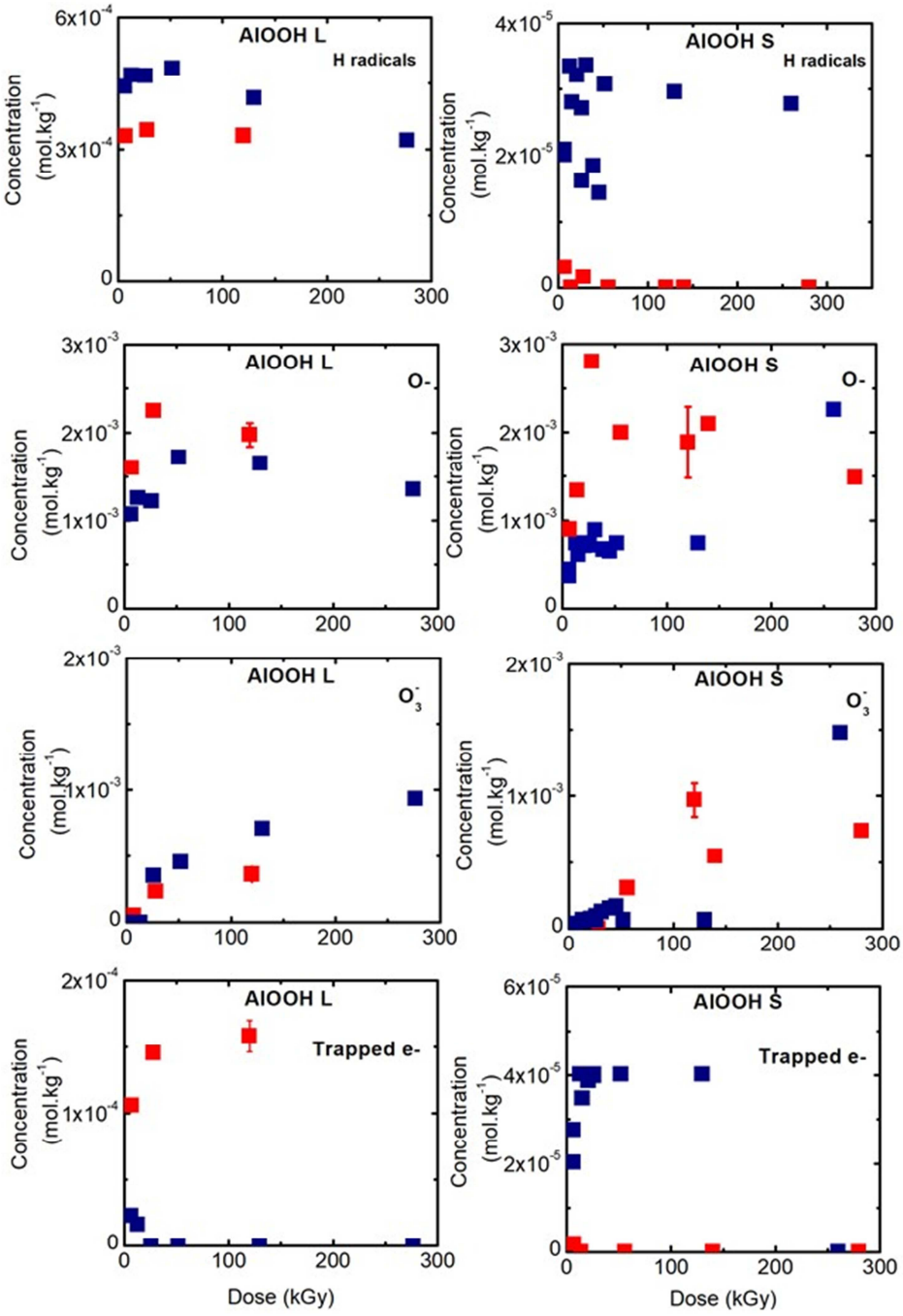

Figure 3. Evolution of the concentration of H radicals, O^-, O_3^- and electrons plotted with respect to dose.

At 77K, O^- is also the major species formed, with G values between 7 and 8 molecules/100eV for AlOOH L and AlOOH S. The ionization process is here more efficient than in water where the initial yield in holes was recently revaluated to 4.8 molecules/100eV.[29] The most

straightforward explanation is the lower band gap of hydroxide materials (4,5 eV),[30] which is very near from the ZrO_2 band gap and much lower than that of water (>6.9 eV).[31] As the Electron-Hole-pair-creation energy is approximatively 3 times the band gap, we can expect the formation of 7.5 holes per 100 eV.[32]

Trapped H atoms are observed in both large particles and small ones at 77K (Figure 2). Their concentration saturates very quickly with the dose at low temperature, reaching 1mmol/kg for AlOOH L and 0.07 mmol/kg for AlOOH S (Data not shown). It shows that H atoms remain very reactive and thus, their mobility is only marginally lower at liquid nitrogen temperature.[33] Interestingly, no trapped electrons are observed in AlOOH S at this temperature, suggesting that their observation at room temperature might result from the reaction of H atoms with hydroxyl. Therefore, the precursor of trapped electrons in aluminum hydroxides may not be free electrons but rather free H atoms.

$$\mathrm{Al\cdots OH^-} + \mathrm{H} \rightarrow \mathrm{Al\cdots OH_2} + \mathrm{e^-_{trapped}} \qquad \text{Equation 10}$$

The annealing at room temperature of samples irradiated at 77K reveals an important decrease of H atom and oxidative defect signals, a decrease that is more pronounced in small particles than in large ones (Figure 2 and Table 1). Therefore, as the primary creation of defects observed at low temperature does not really depend on particle size, the lower H_2 production in AlOOH S compared to AlOOH L should be attributed to secondary, thermally activated recombination rather than to the initial ionization processes.

We cannot directly conclude on an excitonic transfer in our case, as it was supposed for some oxide surfaces considering exciton migration from the bulk to the surface of hydroxyl/water groups that act as energy traps. In our study, H_2 can come either from the bulk and/or from the surface. However, the low dielectric constant of aluminum hydroxides (<10) may favor excited/excitonic state formation by electron hole pairing.[34] Furthermore, excited/excitonic state formation upon irradiation is easily detected in AlOOH by cathodoluminescence, (see SI Figure S9), with light emission arising from their partial deactivation on anionic vacancies (around 420 nm) and on $\mathrm{O^-}$ defect (around 520 nm).[30]

Our results allow to describe more precisely this excitonic process. The oxidative counterpart of hydrogen production is here unambiguously identified as oxygen centered defects in the material, whereas it is still elusive in the case of oxides. Therefore, the exciton interaction with surface water probably corresponds to an injection of the reductive equivalent in water, while the hole remains in the materials as $\mathrm{O^-}$ or O_3^-.

$$\mathrm{Al\cdots OH^-,\ H_2O} \xrightarrow{\text{exciton}} \mathrm{Al\cdots O^- + H,\ H_2O} \qquad \text{Equation 11}$$

Such a mechanism of exciton dissociation is related to the one observed in laser photoexcited alumina, but in this case, solvated electron were observed.[4] However, we must not forget,

that besides favoring exciton dissociation, surface water probably plays a second role in controlling reactive species diffusion and encounter, as shown by the change in defect patterns between dry and hydrated states, in AlOOH L and AlOOH S.

Conclusions

From all these observations, we can draw lessons concerning the design of good radiation-catalytic materials for H_2 production and have high ionization yields. This ideal material must be easily ionized. It must provide an efficient storage of oxidative species and an optimal crystallite size for reducing/oxidant separation. And of course, it must accept water on its surface that will provide both the additional energy trapping sites, and the proper diffusion channel for reductive species.

Acknowledgements

This work has been supported by CEA, AREVA NC and AREVA TN.
We thank Marie-Noëlle Amiot for EPR access as well as Bruno Boizot for EPR experimental support. We thank Vincent Dauvois and Delphine Durant for their advices and help. We are also grateful to Philippe Zeller. We thank Jean-Jacques Pielawski for his implication in this subject.

References

[1] Lollar BS, Onstott T, Lacrampe-Couloume G, Ballentine C. The contribution of the Precambrian continental lithosphere to global H2 production. Nature. 2014;516:379.
[2] Lin LH, Hall J, Lippmann-Pipke J, Ward JA, Sherwood Lollar B, DeFlaun M, et al. Radiolytic H2 in continental crust: nuclear power for deep subsurface microbial communities. Geochemistry, Geophysics, Geosystems. 2005;6.
[3] Dzaugis,M E. Water radiolysis and chemical production rates near solid-water boundaries. Doctoral dissertation. University of Rhode Island. (2016). https://digitalcommons.uri.edu/cgi/viewcontent.cgi?article=1529&context=oa_diss.
[4] Musat R, Vigneron G, Garzella D, LeCaër S, Hergott JF, Renault JP, et al. Water reduction by photoexcited silica and alumina. Chemical Communications 2010;46:2394-6.
[5] Breslav YA, Kotov A, Pshezhetskii SY. Investigation of the mechanism of radiation-catalytic processes on the synthethic zeolites by the EPR method. Inst. of Physical Chemistry. Moscow: 1967.
[6] Petrik NG, Alexandrov AB, Vall AI. Interfacial energy transfer during gamma radiolysis of water on the surface of ZrO2 and some other oxides. The Journal of Physical Chemistry B 2001;105:5935-44.

[7] LaVerne JA, Tandon L. H2 production in the radiolysis of water on CeO2 and ZrO2. The Journal of Physical Chemistry B 2002;106:380-6.
[8] Skotnicki K, Bobrowski K. Molecular hydrogen formation during water radiolysis in the presence of zirconium dioxide. Journal of Radioanalytical and Nuclear Chemistry 2015;304:473-80.
[9] Yamada R, Kumagai Y, Nagaishi R. Effect of alumina on the enhancement of hydrogen production and the reduction of hydrogen peroxide in the γ-radiolysis of pure water and 0.4 M H2SO4 aqueous solution. international journal of hydrogen energy. 2011;36:11646-53.
[10] Yamada R, Nagaishi R, Hatano Y, Yoshida Z. Hydrogen production in the γ-radiolysis of aqueous sulfuric acid solutions containing Al2O3, SiO2, TiO2 or ZrO2 fine particles. International Journal of Hydrogen Energy. 2008;33:929-36.
[11] Essehli R, Crumière F, Blain G, Vandenborre J, Pottier F, Grambow B, et al. H2 production by γ and He ions water radiolysis, effect of presence TiO2 nanoparticles. International Journal of Hydrogen Energy. 2011;36:14342-8.
[12] Yamada R, Kumagai Y. Effects of alumina powder characteristics on H2 and H2O2 production yields in γ-radiolysis of water and 0.4 M H2SO4 aqueous solution. International Journal of Hydrogen Energy 2012;37:13272-7.
[13] Klett C, Cui Y, Devineau S, Foy E, Dagnelie R, Renault JP. H2 production through oxide irradiation: Comparison of gamma rays and vacuum ultraviolet excitation. International journal of hydrogen energy 2013;38:3889-97.
[14] Ikezoe Y, Sato S, Shimizu S, Nakajima H. Potential of carbon dioxide radiolysis for hydrogen production. International Journal of Hydrogen Energy. 1982;7:539-43.
[15] Vagelatos N, Lurie N, Vroom D, Houston D, Baird R, Rogers V. Application of laser fusion to the radiolytic production of hydrogen. International Journal of Hydrogen Energy. 1978;3:177-201.
[16] JO'M B, Dandapani B, Cocke D, Ghoroghchian J. On the splitting of water. International Journal of Hydrogen Energy. 1985;10:179-201.
[17] Alam M, Miserque F, Taguchi M, Boulanger L, Renault JP. Tuning hydrogen production during oxide irradiation through surface grafting. Journal of Materials Chemistry 2009;19:4261-7.
[18] Kaddissy JA, Esnouf S, Durand D, Saffre D, Foy E, Renault J-P. Radiolytic events in nanostructured aluminum hydroxides. The Journal of Physical Chemistry C 2017;121:6365-73.
[19] Wexler A, Hasegawa S. Relative humidity-temperature relationships of some saturated salt solutions in the temperature range 0 to 50 C. Journal of Research of the National Bureau of Standards 1954;53:19-26.
[20] Greenspan L. Humidity fixed points of binary saturated aqueous solutions. Journal of research of the national bureau of standards 1977;81:89-96.
[21] Kaddissy J. Hydrogen production from irradiated aluminum hydroxide and oxyhydroxide. Doctoral dissertation. Paris Saclay: 2016. https://tel.archives-ouvertes.fr/tel-01531842

[22] Fricke, H. H., J. E, Attix, F. H., Roesch, W.C., Eds. In Radation Dosimetry, 2nd Ed. Academic Press: New York and London 1966;2, 167.
[23] Sutton, H. C. A Calibration of the Fricke Chemical Dosimeter. Phys Med Biol 1956; 1, 153.
[24] Haschke, J. M.; Ricketts, T. E., Adsorption of Water on Plutonium Dioxide. J Alloys Compd 1997; 252, 148-156.
[25] Rotureau P, Renault J, Lebeau B, Patarin J, Mialocq JC. Radiolysis of confined water: molecular hydrogen formation. ChemPhysChem 2005;6:1316-23.
[26] Yurik T, Ionova G, Barsova L, Spitsyn V. ESR investigation of hydrogen atoms stabilized in γ-irradiated alkaline earth hydroxides. Radiation effects 1988;106:87-98.
[27] Griscom DL. Diffusion of radiolytic molecular hydrogen as a mechanism for the post-irradiation buildup of interface states in SiO2-on-Si structures. Journal of Applied Physics 1985;58:2524-33.
[28] Lousada CM, Soroka IL, Yagodzinskyy Y, Tarakina NV, Todoshchenko O, Hänninen H, et al. Gamma radiation induces hydrogen absorption by copper in water. Scientific reports 2016;6:24234.
[29] El Omar AK, Schmidhammer U, Jeunesse P, Larbre J-P, Lin M, Muroya Y, et al. Time-dependent radiolytic yield of OH• radical studied by picosecond pulse radiolysis. The Journal of Physical Chemistry A 2011;115:12212-6.
[30] Alemi A, Hosseinpour Z, Dolatyari M, Bakhtiari A. Boehmite (γ-AlOOH) nanoparticles: Hydrothermal synthesis, characterization, pH-controlled morphologies, optical properties, and DFT calculations. Physica status solidi (b) 2012;249:1264-70.
[31] Fang C, Li W-F, Koster RS, Klimeš J, Van Blaaderen A, Van Huis MA. The accurate calculation of the band gap of liquid water by means of GW corrections applied to plane-wave density functional theory molecular dynamics simulations. Physical Chemistry Chemical Physics 2015;17:365-75.
[32] Alig R, Bloom S. Electron-hole-pair creation energies in semiconductors. Physical review letters 1975;35:1522.
[33] Markland TE, Habershon S, Manolopoulos DE. Quantum diffusion of hydrogen and muonium atoms in liquid water and hexagonal ice. The Journal of chemical physics 2008;128:194506.
[34] Abram A, Eršte A, Dražić G, Bobnar V. Structural and dielectric properties of hydrothermally prepared boehmite coatings on an aluminium foil. Journal of Materials Science: Materials in Electronics 2016;27:10221-5.